



ARTICLE

Zika NS1-induced ER remodeling is essential for viral replication

Yali Ci^{1,2}, Zhong-Yu Liu^{3,4}, Na-Na Zhang⁴, Yuqiang Niu⁵, Yang Yang^{1,2}, Caimin Xu^{1,2}, Wei Yang⁵, Cheng-Feng Qin^{4,6} , and Lei Shi^{1,2} 

Zika virus (ZIKV), a recently emerged member of the flavivirus family, forms replication compartments at the ER during its lifecycle. The proteins that are responsible for the biogenesis of replication compartments are not well defined. Here, we show that Zika nonstructural protein 1 (NS1)-induced ER remodeling is essential for viral replication. NS1 expressed in the ER lumen induced ER perinuclear aggregation with an ultrastructure resembling that of the replication compartment. Data from model membrane system indicated that the membrane-binding and membrane-remodeling properties of NS1 depend on its hydrophobic insertion into the membrane. These findings demonstrate that NS1 plays a crucial role in flavivirus replication compartment formation by remodeling the ER structure.

Introduction

Flavivirus replication occurs in membranous compartments called replication compartments that are derived from the ER (Paul and Bartenschlager, 2015; Ravindran et al., 2016). The replication compartment is the structural foundation for viral replication complex assembly and RNA synthesis. This distinct ER architecture is characterized by convoluted membrane networks and vesicle packets (VPs) derived from ER invagination, which is the cellular hallmark of flavivirus replication (Cortese et al., 2017; Welsch et al., 2009). Although the architecture of the replication compartment has been described, the underlying mechanism is still obscure.

The biogenesis of the flavivirus replication compartment is essentially a process of ER membrane remodeling. Membrane remodeling is associated with many physiological processes, such as intracellular trafficking and maintenance of organelle morphology. The usual ER membrane deformation is budding toward cytoplasm to generate vesicles for transportation and communication with other organelles (Miller and Barlowe, 2010), but ER invagination is rare under physiological conditions. Vesicle budding from the ER could be ascribed to host factors, but these factors have seldom been found to induce ER invagination. Therefore, it is rational to attribute ER invagination during flavivirus infection to viral proteins. However, the proteins responsible for the creation of viral replication compartment and underlying mechanisms remain unclear.

Flaviviruses are positive single-strand RNA viruses whose genomes encode three structural proteins (capsid, prM/M, and envelope) and seven nonstructural (NS) proteins (NS1, NS2A, NS2B, NS3, NS4A, NS4B, and NS5; Apte-Sengupta et al., 2014; Selisko et al., 2014). The three structural proteins are components of the virus particle, while the NS proteins are responsible for viral replication. Among these replication-associated NS proteins, NS3 and NS5 are enzymes with protease, RNA helicase, and RNA-dependent RNA polymerase activities. Four transmembrane proteins on the ER, NS2A, NS2B, NS4A, and NS4B, are considered as scaffolds for replication complex assembly (Chambers et al., 1990). The NS1 protein is the first NS protein and has been demonstrated to be essential for viral replication.

Flavivirus NS1 forms dimer localized in the ER lumen and can be secreted to extracellular milieu. Multiple functions of NS1 have been reported, suggesting its role as a cofactor via interacting with other viral proteins to facilitate viral replication (Chen et al., 2015; Glasner et al., 2018; Gutsche et al., 2011; Liu et al., 2017a; Watterson et al., 2016). Moreover, NS1 has been reported as a membrane-binding protein (Akey et al., 2014; Gutsche et al., 2011), whereas no direct evidence declares the relationship between its membrane association property and its essentiality in viral replication. Thus, the genuine function of NS1 in flavivirus replication is still a mystery, and whether its membrane-binding property is involved remains obscure.

¹State Key Laboratory of Medical Molecular Biology, Institute of Basic Medical Sciences, Chinese Academy of Medical Sciences and School of Basic Medicine, Peking Union Medical College, Beijing, China; ²Department of Biochemistry and Molecular Biology, Institute of Basic Medical Sciences, Chinese Academy of Medical Sciences and School of Basic Medicine, Peking Union Medical College, Beijing, China; ³Guangzhou Eighth People's Hospital, Guangzhou Medical University, Guangzhou, China; ⁴State Key Laboratory of Pathogen and Biosecurity, Beijing Institute of Microbiology and Epidemiology, Beijing, China; ⁵Institute of Pathogen Biology, Chinese Academy of Medical Sciences, Beijing, China; ⁶The First Hospital of Jilin University, Changchun, China.

Correspondence to Lei Shi: shilei@ibms.pumc.edu.cn; Cheng-Feng Qin: qincf@bmi.ac.cn; Wei Yang: wyang@ipb.pumc.edu.cn.

© 2019 Ci et al. This article is distributed under the terms of an Attribution-Noncommercial-Share Alike-No Mirror Sites license for the first six months after the publication date (see <http://www.rupress.org/terms/>). After six months it is available under a Creative Commons License (Attribution-Noncommercial-Share Alike 4.0 International license, as described at <https://creativecommons.org/licenses/by-nc-sa/4.0/>).

Here, we found that NS1 in ER lumen remodels ER membrane, creating a replication compartment-like structure. Using a model membrane system, we found that Zika virus (ZIKV) NS1 bound to liposomes and induced tubules protruding from liposomes in vitro. NS1 is essential to reorganize ER structure through insertion of its hydrophobic regions into ER membranes to generate a replication compartment-like structure, thus determining viral replication. This work reveals the critical role of NS1 in flavivirus replication and the underlying mechanism of ER reorganization by ZIKV.

Results

NS1 induces ER remodeling

ZIKV, a member of the Flavivirus family, which also includes yellow fever virus (YFV), dengue virus (DENV), West Nile virus, Japanese encephalitis virus, etc., emerged in 2015 and raised public concerns due to its associated neurological symptoms, such as neonatal microcephaly and Guillain-Barré syndrome. ZIKV also caused severe testis damage in mouse models (Ma et al., 2017; Tang et al., 2016; Wikan and Smith, 2016; Yuan et al., 2017). As expected, ZIKV infection induced perinuclear ER aggregation (Fig. 1 A). Upon ultrastructural examination, the classic architecture of the flavivirus replication compartment could be observed (Fig. S1, A and B). To study the viral replication process, we introduced ZIKV replicon here. ZIKV replicon construct contains all replication-related NS proteins coding sequences as well as 5' and 3' UTR, while those of structural proteins are replaced by a luciferase gene. With transfection of replicon RNA into cells, similar VPs were observed (Fig. 1 B; Li et al., 2018), suggesting that these vesicles are replication-related and induced by viral NS proteins. To clarify the roles of these NS proteins in generating replication compartment, we expressed them in cells and examined ER morphology. The viral RNA polymerase, ZIKV NS5 protein, which localized in both nucleus and cytoplasm, did not alter ER morphology (Fig. S1 C). NS2A, 2B, 4A, and 4B are multi-transmembrane proteins residing on ER membrane, and some of them have been reported to modify membrane structure (Miller et al., 2007; Roosendaal et al., 2006). NS3 has protease activity to cleave viral polyprotein into individual ones. We expressed NS2A-NS4B (including NS2A, 2B, 3, 4A, and 4B) as a single-chain polypeptide with an N-terminal enhanced ascorbate peroxidase 2 (APEX2) tag. APEX2-catalyzed DAB reaction generates EM contrast and is used to elucidate subcellular localization of a protein of interest or the structure of a specific subcellular compartment. Once expressed, NS2A-4B polypeptide would be processed by NS2B-3 protease and host protease, as happens in the case of ZIKV infection. Although there is evidence showing that NS4A/B rearranges cytosolic membrane, we found that NS2A-4B did not induce replication compartment-like structures (Fig. 1, C and D).

Flavivirus NS1 has been known to be involved in viral replication for decades. Earlier studies found that deletion or mutation of YFV NS1 resulted in the defect of viral RNA accumulation, implying its essential role in RNA synthesis (Muylaert et al., 1997). To explore ZIKV NS1 function in viral replication, we performed a ZIKV replicon luciferase assay. We

constructed a ZIKV Δ NS1 replicon by deleting a large fragment of NS1 (11–271 residues). Luciferase activity of WT or Δ NS1 replicon was examined 10 h after transfection (representing transcribed replicon RNA) or 36 h after transfection (representing self-replication of replicon RNA). WT ZIKV replicon successfully replicated in the cell as a robust luciferase activity was detected at 36 h after transfection. However, Δ NS1 replicon showed little luciferase activity at 36 h after transfection, indicating the failure of replication (Fig. 1 E). To confirm viral RNA synthesis was blocked upon NS1 deletion, immunostaining was performed with an anti-double stranded RNA (dsRNA) antibody. WT ZIKV replicon is competent to replicate by itself, producing dsRNA intermediate products around the ER at 24 h after transfection, while no viral dsRNA signal was observed in cells transfected with Δ NS1 ZIKV replicon RNA (Fig. 1 F). These data suggested that NS1 deletion blocked viral RNA synthesis, which is consistent with results of YFV (Lindenbach and Rice, 1997; Muylaert et al., 1997).

As an ER luminal protein, NS1 is spatially separated from both the viral RNA and the viral RNA synthesizing complex by the ER membrane. Thus, how NS1 affects RNA amplification without direct contact with substrates and enzymes is unclear. Upon ZIKV infection, we examined the location of NS1 and found that it was enriched at the ER aggregation site (Fig. 1, G and H), where the virus replication compartments localized, suggesting an association between NS1 and the replication compartment. Considering its natural location in the ER lumen, we expressed NS1 in the cytoplasm (without a signal sequence, –ss) or ER lumen (with a signal sequence, +ss). NS1 markedly induced effective ER perinuclear aggregation only when it was expressed in the ER lumen (+ss); the effect was not observed for cytosolic NS1 (–ss; Fig. 1, I and J). In addition to spatial dependence, dose dependence was also observed, as higher expression level of NS1 caused more prominent ER aggregation (Fig. 1 I, arrows point to cells with higher level of NS1 expression). Similarly, DENV NS1 also exhibited ER remodeling activity (Fig. S2), suggesting a shared NS1-dependent ER remodeling strategy among flaviviruses. Taken together, our results suggest that NS1 is capable of inducing ER remodeling and may participate in the construction of the ZIKV replication compartment.

NS1 binds to the membrane through hydrophobic insertion

To test the membrane-binding activity of NS1, we performed a liposome cofloating assay (Tucker et al., 2004). The result of liposome cofloating assay manifested the membrane-binding capacity of NS1 (Fig. 2, A and B). Among known membrane-binding patterns, hydrophobic insertion is a common way for protein–membrane interaction. Based on its structure, dimeric NS1 possesses a membrane-associated face. Three hydrophobic regions on the membrane-associated face, the β -roll, the greasy finger (GF), and the wing flexible loop, are assumed to insert into the lipid membrane (Fig. 2 C), but there is a lack of direct evidence (Akey et al., 2014; Brown et al., 2016; Xu et al., 2016). To examine the membrane insertion of each hydrophobic region, we performed a doxyl-quenching assay using peptides carrying single tryptophan (Trp) residues derived from these hydrophobic regions. Upon incubation of single Trp-containing peptides

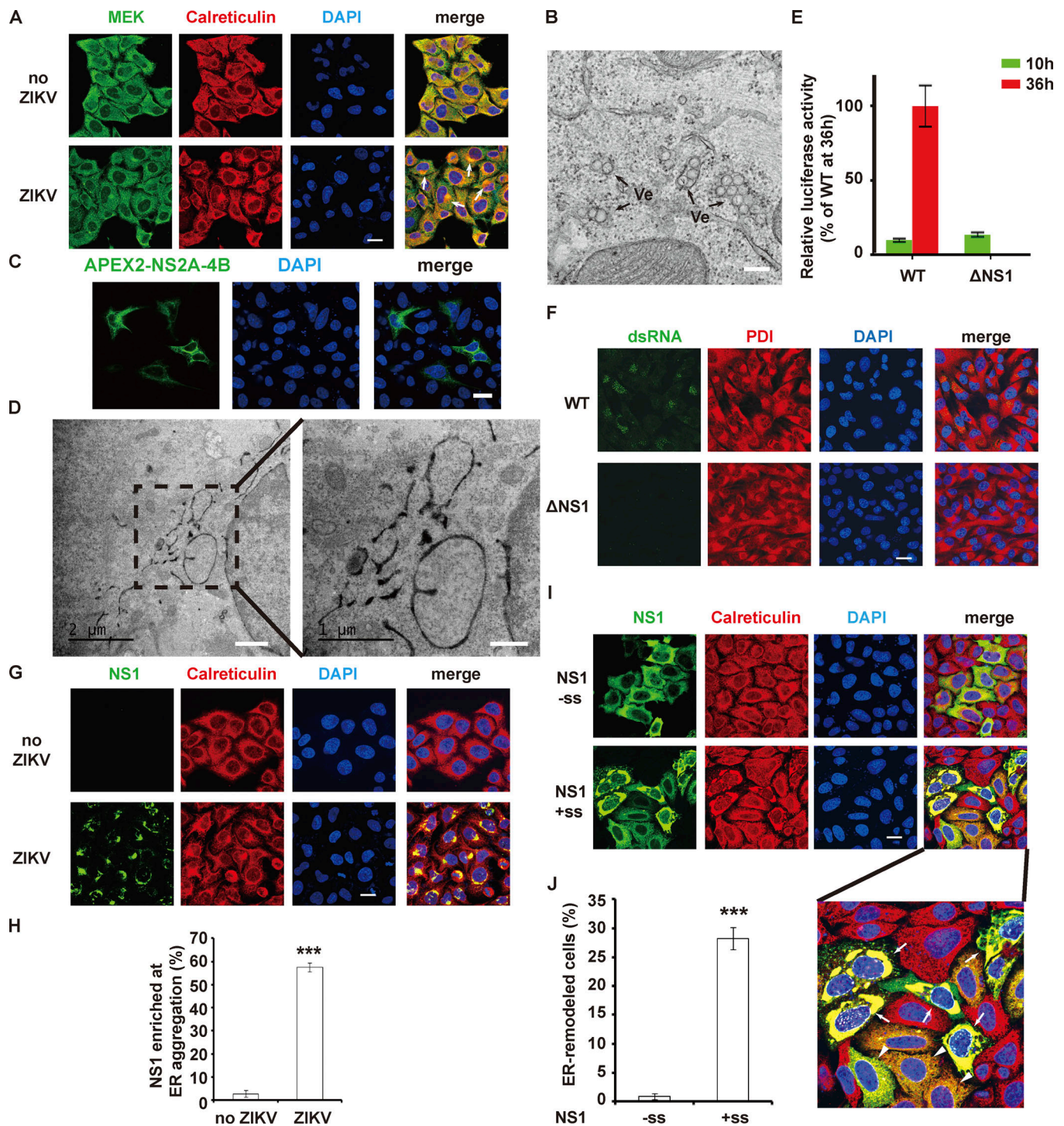


Figure 1. NS1 is essential for building replication compartment by ER remodeling. (A) ER morphology in ZIKV-infected HeLa cells. The arrows point to ER aggregation, indicating the replication compartments. Green, MEK (cytosolic marker); red, calreticulin (ER marker). (B) EM image showing ZIKV replicon-induced VPs in BHK-21 cells, which is the characteristic structure of replication compartments. Ve, vesicle. Scale bar, 200 nm. (C and D) ER morphology of APEX2-NS2A-4B-expressed cells. The polypeptide containing ZIKV NS2A, 2B, 3, 4A, and 4B was expressed in HeLa cells, and ER morphology was examined by confocal microscope (C) or EM (D). Scale bars in D, 1 μ m (left panel), 500 nm (right panel). (E) ZIKV replicon luciferase assay. *Renilla* luciferase activity was measured at 10 h and 36 h after transfection of cells with WT or mutated ZIKV replicon RNA. (F) dsRNA intermediate detection in replicon transfected cells. WT or Δ NS1 replicon-transfected BHK-21 cells were stained with J2 antibody (green, anti-dsRNA antibody) and anti-PDI antibody (red, ER marker). (G and H) NS1 is enriched at the site of ER aggregation in ZIKV-infected HeLa cells. ZIKV-infected HeLa cells were stained with antibodies specific for ZIKV NS1 (green) and calreticulin (red). The percentage was defined as the ratio of the number of cells with NS1 enrichment at ER aggregation sites to the number of NS1-positive cells. (I and J) Expression of ZIKV NS1 in ER lumen induces ER remodeling. Myc-tagged cytosolic ZIKV NS1 (without signal sequence, -ss) and ER lumen-located NS1 (led by signal sequence, +ss) were stained with anti-Myc (green) and calreticulin (red) antibodies. A higher-magnification image is shown below. The arrows indicate ER aggregation in cells expressing high NS1 levels. The arrowheads indicate ER morphology in cells expressing less NS1. The percentage was defined as the ratio of the number of cells with ER remodeling to the number of NS1-expressing cells. Scale bars, 20 μ m for the confocal images in A, C, F, G, and I. The data are presented as the mean \pm SEM. The P values are obtained from a two-tailed t test. ***, P < 0.001.

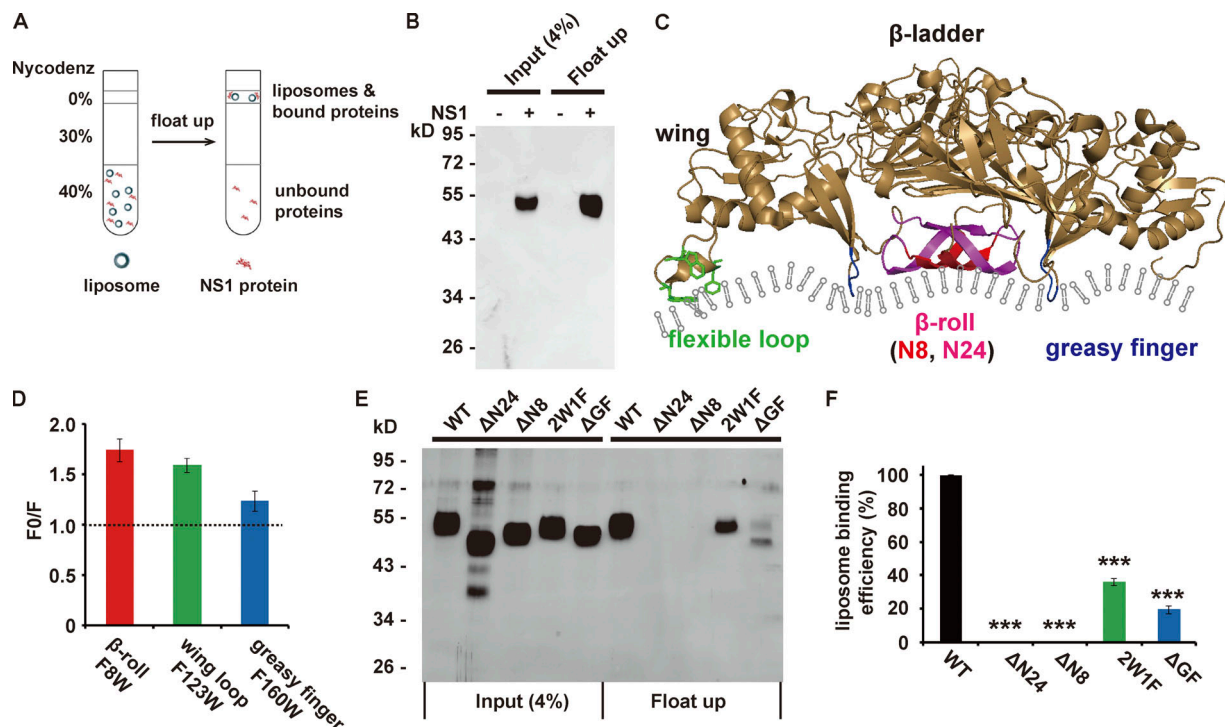


Figure 2. ZIKV NS1 binds to the membrane via hydrophobic insertion. (A) Schematic diagram of the liposome cofloat assay. The ZIKV NS1 protein was incubated with liposomes (~100 nm diameter) for 4 h at 37°C, and the protein–liposome mixture was then ultracentrifuged against 40%, 30%, and 0% Nycodenz gradients. Membrane-bound NS1 cofloated with liposomes, whereas unbound NS1 remained on the bottom. (B) NS1 cofloats with liposomes. Input and cofloating samples of NS1 were analyzed by silver staining. (C) Structure of the ZIKV NS1 dimer (PDB 5k6k). The hydrophobic membrane-binding regions are marked in different colors: red (eight N-terminal residues of the β-roll), red plus pink (24 N-terminal residues of the β-roll), green (wing flexible loop; three hydrophobic residues, W115, W118, and F123, are shown as sticks), and blue (GF). (D) Doxyl quenching of Trp in peptides derived from NS1 hydrophobic regions. Peptides with a single Trp were mixed with 12-doxyl-labeled (F) or unlabeled (F0) liposomes, and the fluorescence of Trp was monitored at 330 nm. The quenching level is presented as F0/F. (E and F) Liposome-binding activity of WT and mutated NS1. (E) Silver-stained gel for input and cofloated NS1. (F) Quantification of the cofloating assay. Liposome-binding efficiency was defined as the percentage of cofloated NS1 to the input, and the binding efficiency of WT NS1 was set to 100%. The data are the mean ± SEM. The P values are obtained from a two-tailed t test. ***, P < 0.001.

with liposomes labeled with 12-doxyl-PC, the fluorescence of Trp will be quenched when the peptides insert into the lipid bilayer. All three peptides showed weaker fluorescence after incubation with doxyl-labeled liposomes, supporting their membrane insertion (Fig. 2 D). We then introduced deletions or point mutations into NS1 and examined their influence on NS1 association with the lipid membrane (Fig. S3). The GF deletion (ΔGF, 159–163 residues deletion) and wing flexible loop mutation (2W1F, W115A/W118A/F123A) resulted in prominent loss of liposome-binding capacity. ΔN24 (deletion of the 24 N-terminal residues in β-roll) and ΔN8 (deletion of the 8 N-terminal residues in β-roll) almost abolished liposome binding in the cofloating assay (Fig. 2, E and F). Given the strong defect upon N-terminal deletion, we also mutated two hydrophobic residues, V6 and F8, to alanine; both mutations partially impaired liposome-binding capacity, implying that these sites are involved in membrane insertion (Fig. S4). Thus, we conclude that NS1 binds to liposomes by hydrophobic membrane insertion.

NS1 remodels membrane structure in vitro and in vivo

Considering the alteration of ER morphology in NS1-expressed cells and the membrane association property of NS1 via hydrophobic insertion, we assumed NS1 might affect membrane

curvature. We coincubated liposomes with NS1 proteins and examined liposome structure by EM upon negative staining. We found that WT NS1 induced long and thin tubules protruding from liposomes, while ΔN8 mutant treatment induced fewer and shorter ones on a few liposomes (Fig. 3, A and B). This finding implied that NS1 changes membrane curvature depending on membrane binding and hydrophobic insertion. Likely, ER lumen-localized NS1 may possibly induce negative curvature (away from the cytoplasm) on ER membrane as invaginated vesicles (Jarsch et al., 2016), constructing the flavivirus replication compartments. To confirm that this membrane-remodeling mechanism is the basis of NS1-induced ER reorganization, we expressed WT or mutated NS1 in cells. At similar expression levels, the ΔGF and 2W1F mutants induced much less perinuclear aggregation than WT NS1, while ΔN8 could hardly change ER morphology (Fig. 3, C–E). These in vitro and in vivo results suggest that NS1 is a robust membrane curvature inducer involved in ER remodeling and essential for flavivirus replication.

NS1 remodels ER resembling viral replication compartment

As shown in Fig. 1 I, NS1 induced ER aggregation in cells. To examine the ultrastructure of NS1-induced ER aggregation, we

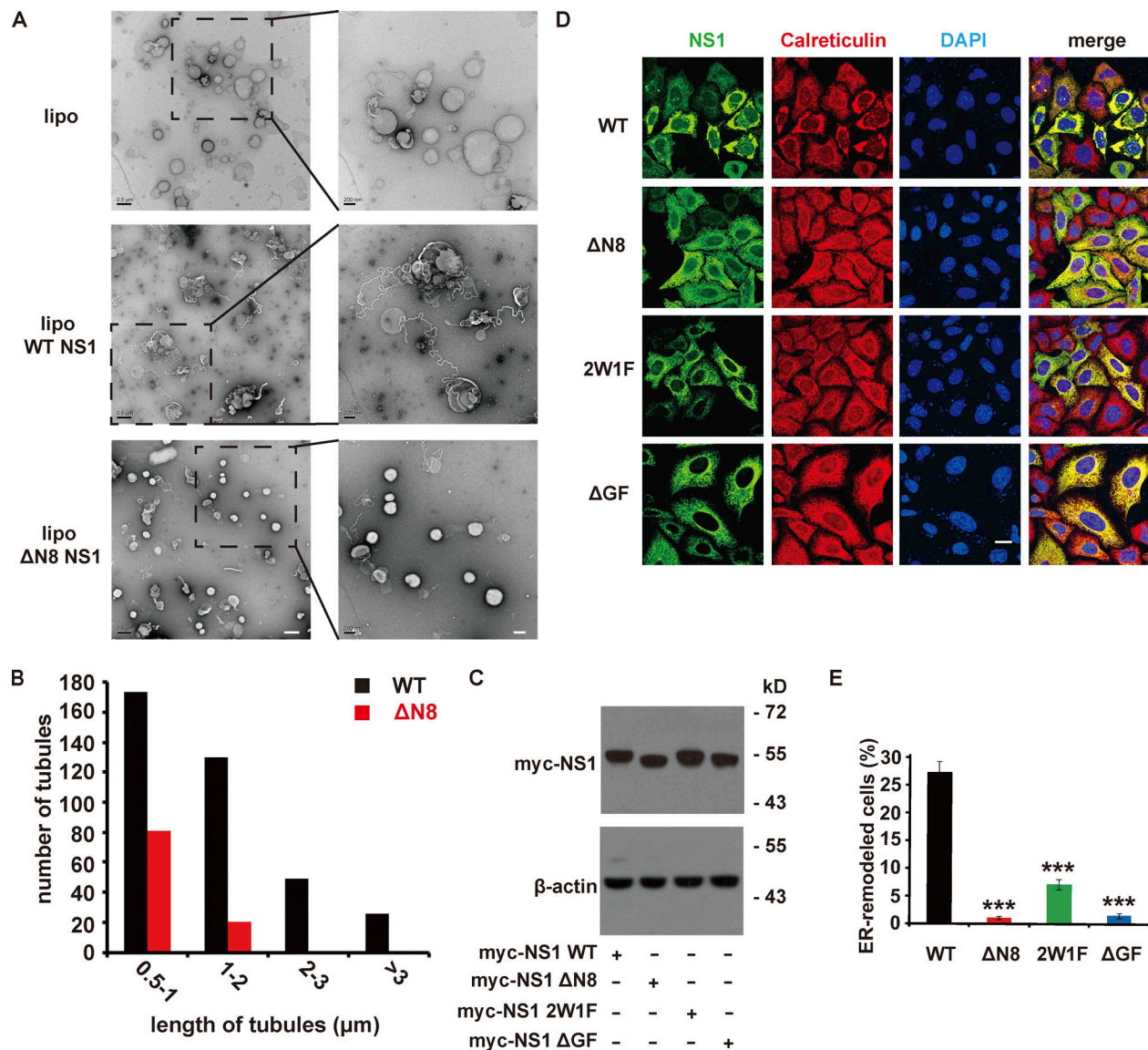


Figure 3. ZIKV NS1 remodels membrane structure in vitro and in vivo. (A) EM imaging of liposomes (lipo) with or without NS1 proteins incubation. Liposomes (~ 400 nm diameter) were incubated with NS1 proteins for 2 h at RT and then analyzed by EM after negative staining. Scale bar, left panel, 500 nm; right panel, 200 nm. (B) The length distribution of tubules induced by NS1 proteins. The length of tubules on liposomes was measured, and the number of tubules with different lengths was counted. (C) Expression of Myc-tagged WT or mutated ZIKV NS1 in HeLa cells. HeLa cells were transfected with WT or mutated ZIKV NS1. At 24 h after transfection, NS1 was detected by Western blotting with an anti-Myc antibody. (D) HeLa cells expressing Myc-tagged WT or mutated NS1 were stained with antibodies against Myc-tag (green) or calreticulin (red). Scale bar, 20 μm . (E) Percentage of cells with ER remodeling mediated by WT or mutated NS1. The percentage is defined as the ratio of cells with ER remodeling to NS1-expressing cells. The data are the mean \pm SEM. The P values are obtained from a two-tailed *t* test. ***, *P* < 0.001.

observed ER morphology by EM. Upon NS1 expression, many cells displayed quite different ER morphology from the regular tubular structures, with convoluted ER networks and crowded vesicles (Fig. 4 A). However, such structure is rarely observed in the cells transfected with ΔN8 NS1 (Fig. 4 B). To label NS1-expressing cells and illustrate NS1 subcellular localization in EM imaging, an APEX2 tag was fused to the C terminus of NS1. DAB reaction products marked NS1-localized ER lumen (Fig. 4, C–F). Furthermore, we observed vesicles encircled by dark reaction products, indicating that those are ER invagination. The average diameter of these vesicles was 86.19 ± 1.68 nm, close to the reported diameter of vesicles from flavivirus replication

(~ 90 nm; Fig. 4 E), whereas ER in the cells expressing ΔN8 NS1 retained tubular morphology (Fig. 4, D and F).

NS1 functions as a dimer

Flavivirus NS1 forms a dimer in the crystal structure (Akey et al., 2014), but it is unclear whether NS1 functions as a dimer to remodel ER. To examine the interactions between ZIKV NS1 proteins in cells, we coexpressed Flag-NS1 and Myc-NS1 and performed a coimmunoprecipitation assay. The data revealed an interaction between these proteins, confirming that NS1 forms a dimer in cells (Fig. 5, A and B). Flag-tagged WT NS1 interacted with Myc-tagged NS1 mutants with mutation in

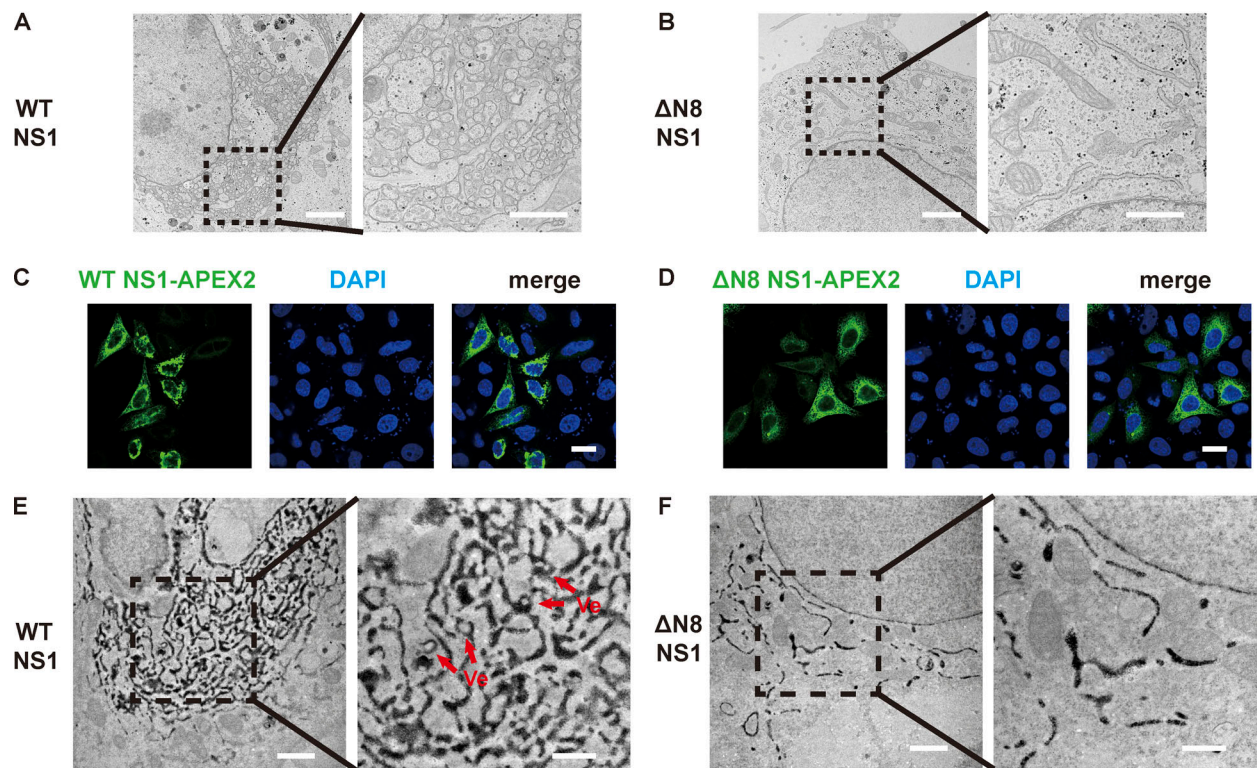


Figure 4. ZIKV NS1 remodels ER resembling viral replication compartments. (A and B) Ultrastructure of ER in WT (A) or ΔN8 (B) NS1-transfected HeLa cells. WT NS1-transfected cells exhibit convoluted ER networks and crowded vesicles, while ΔN8 NS1-transfected cells show a normal ER structure. Right panel, High magnification of the indicated area. Scale bars, 2 μm (left panel), 1 μm (right panel). (C and D) WT or ΔN8 NS1-APEX2 expression and localization in HeLa cells. NS1-APEX2 with a signal sequence was expressed in HeLa cells and the distribution of WT (C) or ΔN8 (D) NS1-APEX2 was analyzed by confocal microscopy. Scale bar, 20 μm. (E and F) ER morphology of WT or ΔN8 NS1-APEX2-expressed HeLa cells. Ultrastructure of ER in WT (E) or ΔN8 (F) NS1-APEX2-expressed cells was analyzed by electron microscope. Arrows point to invaginated vesicles on ER. Scale bars, 1 μm (left panel), 500 nm (right panel).

NS1 hydrophobic regions, suggesting these regions are unrelated to NS1 dimerization (Fig. 5, A and B). However, there was less ER aggregation in the cells coexpressing WT and mutant NS1 than that in the cells expressing WT NS1 alone, indicating that NS1 mutants interfered with WT NS1-induced ER remodeling (Fig. 5, C and D). Consistently, cotransfection of WT and ΔN8 NS1 replicons showed weaker replication activity than cotransfection of WT and ΔNS1 replicons (Fig. 5 E). These data imply that NS1 functions as a dimer and the mutants have a dominant negative effect on ER remodeling and viral replication.

The NS1-induced replication compartment is the structural basis of viral replication

Our data and previous studies revealed the essential role of NS1 in flavivirus replication. To explore whether NS1 membrane-binding and remodeling property is directly related to ZIKV replication, we prepared several NS1-mutated ZIKV replicons and examined their self-replication by the luciferase assay. Compared with the WT replicon, which showed a robust luciferase signal at 36 h after transfection, the ΔN8 NS1 replicon showed little luciferase activity, similar to the replication-incompetent replicon carrying the NS5 GAA mutation (residues 664–666, GDD to GAA, RNA polymerase-inactive mutant; Fig. 6 A). Mutations in NS1 hydrophobic regions (β-roll or GF),

including V6A/F8A, F160A/F163A, and V6A/F8A/F160A/F163A, also severely blocked viral replication (Fig. S5). The abolishment of viral replication by mutation in hydrophobic regions suggested that the function of NS1 in viral replication relies on its interaction with the membrane. A few mutagenesis screens have indicated the importance of the N-terminal regions of NS1, but the mechanisms remained unknown (Fulton et al., 2017; Muylaert et al., 1997); these mechanisms can now be explained by our findings. Mutations in the N terminus, particularly in the β-roll, disrupted the interaction between NS1 and the ER membrane, thus blocking viral replication. Furthermore, dsRNA staining indicated the viral RNA synthesis in cells transfected with the WT replicon, whereas the dsRNA signal was minimal in cells transfected with ΔN8 NS1 replicon, consistent with the luciferase assay results in Fig. 6 A (see also Fig. 6 B). This finding confirmed NS1 membrane binding and remodeling is essential for viral RNA amplification. Unsurprisingly, the lack of dsRNA synthesis in the NS5 GAA mutant was due to inactivity of RNA polymerase. However, the elimination of RNA replication coming from NS1 mutation was due to the impairment of association between NS1 and lipid membrane.

Considering the ER-remodeling activity of NS1, we assumed that failure to create a proper replication compartment was responsible for the replication blockage caused by NS1 mutation. Ultrastructural imaging showed that WT replicons induced VPs

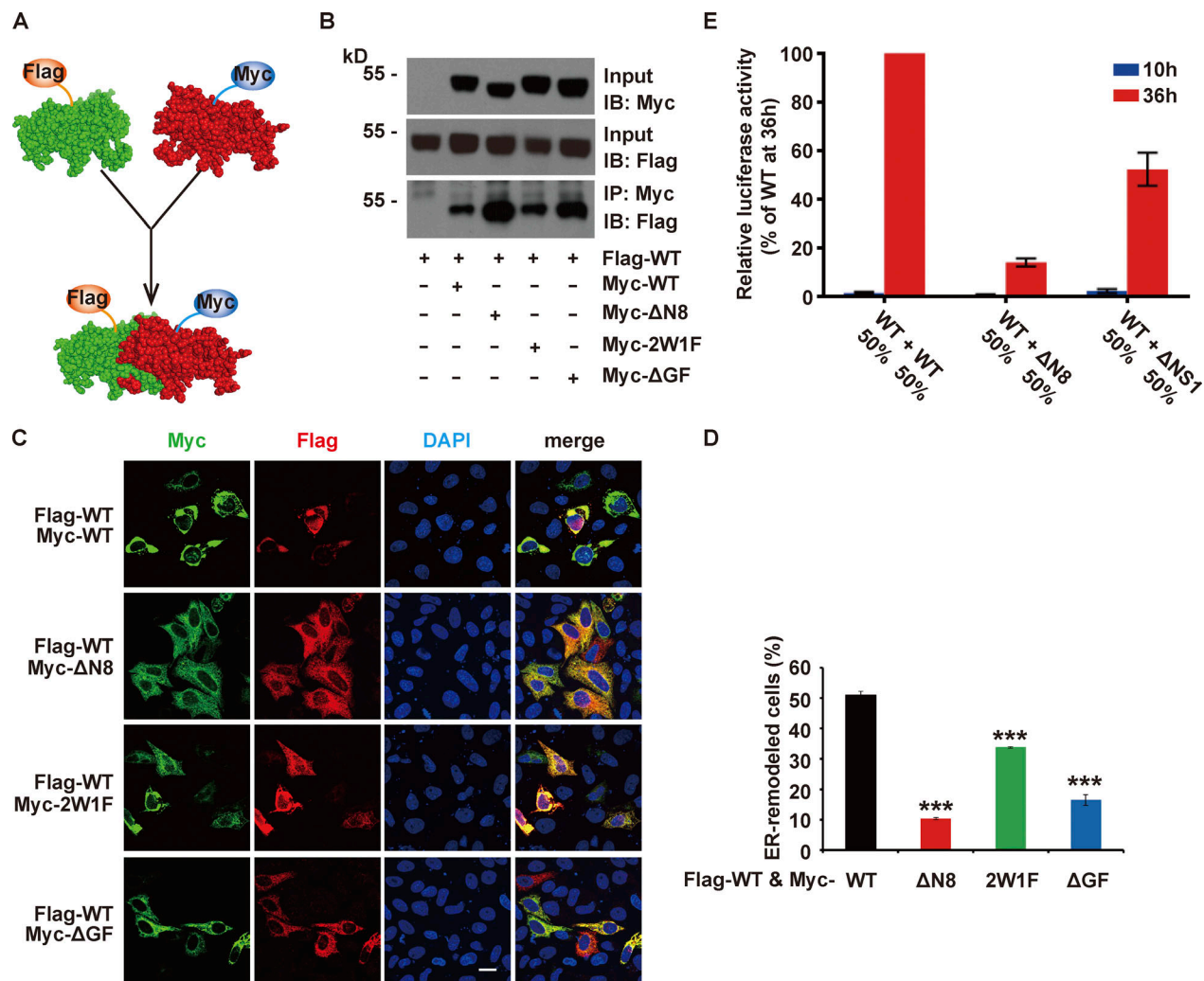


Figure 5. NS1 functions as a dimer. (A) Schematic showing the hetero-dimerization between Flag-tagged WT and Myc-tagged NS1. (B) Dimerization of NS1 proteins with different tags in cotransfected cells. Flag-tagged WT NS1 and Myc-tagged WT or mutated NS1 was coexpressed in HeLa cells. Immunoprecipitation (IP) was performed using a Myc antibody. The proteins precipitated by Myc-tagged NS1 were immunoblotted (IB) with a Flag antibody. (C and D) NS1 mutants interfere with WT NS1-induced ER remodeling. Cells were cotransfected with Myc-tagged WT or mutated NS1 and Flag-tagged WT NS1, and then immunofluorescence was examined. ER morphology is indicated by NS1 staining. Scale bar, 20 μ m. (D) The percentage of ER-remodeled cells was defined as the ratio of the number of cells with ER remodeling to the number of cotransfected cells (green and red double-labeled). The data are presented as the mean \pm SEM. The P values are obtained from a two-tailed t test. ***, $P < 0.001$. (E) NS1-mutated replicons interfere with the luciferase activity of WT replicons. BHK-21 cells were cotransfected with WT and NS1-mutated replicons, and the luciferase activity was measured at 10 h and 36 h after transfection.

at the ER, while such structures were rarely found in cells transfected with the Δ N8 NS1 replicon, indicating that ER reorganization by NS1 is indispensable for biogenesis of the replication compartments (Fig. 6 C). Then, we introduced these replication-deficient mutations, Δ NS1, Δ N8, and NS5 GAA, into ZIKV-infectious cDNA clones to detect their impacts on the production of recombinant ZIKV (rZIKV; Shan et al., 2016). Consistent with the above results, little viral RNA was produced from infectious clones carrying these mutations (Fig. 6 D). Furthermore, the Δ NS1, Δ N8 NS1, and NS5 GAA mutants could not produce infectious rZIKV (Fig. 6 E). Conclusively, ZIKV NS1-induced ER remodeling is the basis of replication compartment biogenesis, and its deficiency results in abolishment of viral replication and production.

Discussion

Membranous compartment for the replication of positive-strand RNA viruses

Positive-strand RNA viruses constitute a large class of viruses, many of which are pathogens causing serious concerns. Fascinatingly, most of these viruses generate special membranous structures in the cell for viral replication (den Boon and Ahlquist, 2010; Hsu et al., 2010). These structures are usually derived from intracellular membranous organelles, such as the ER, mitochondria, and Golgi apparatus, and possess vesicle-like morphology; however, they are not completely sealed, but connected with cytoplasm through a channel. The characteristic structure functions as the platform for replication complex assembly and protects the templates, machines, and products from being recognized and attacked by the host. Meanwhile, it

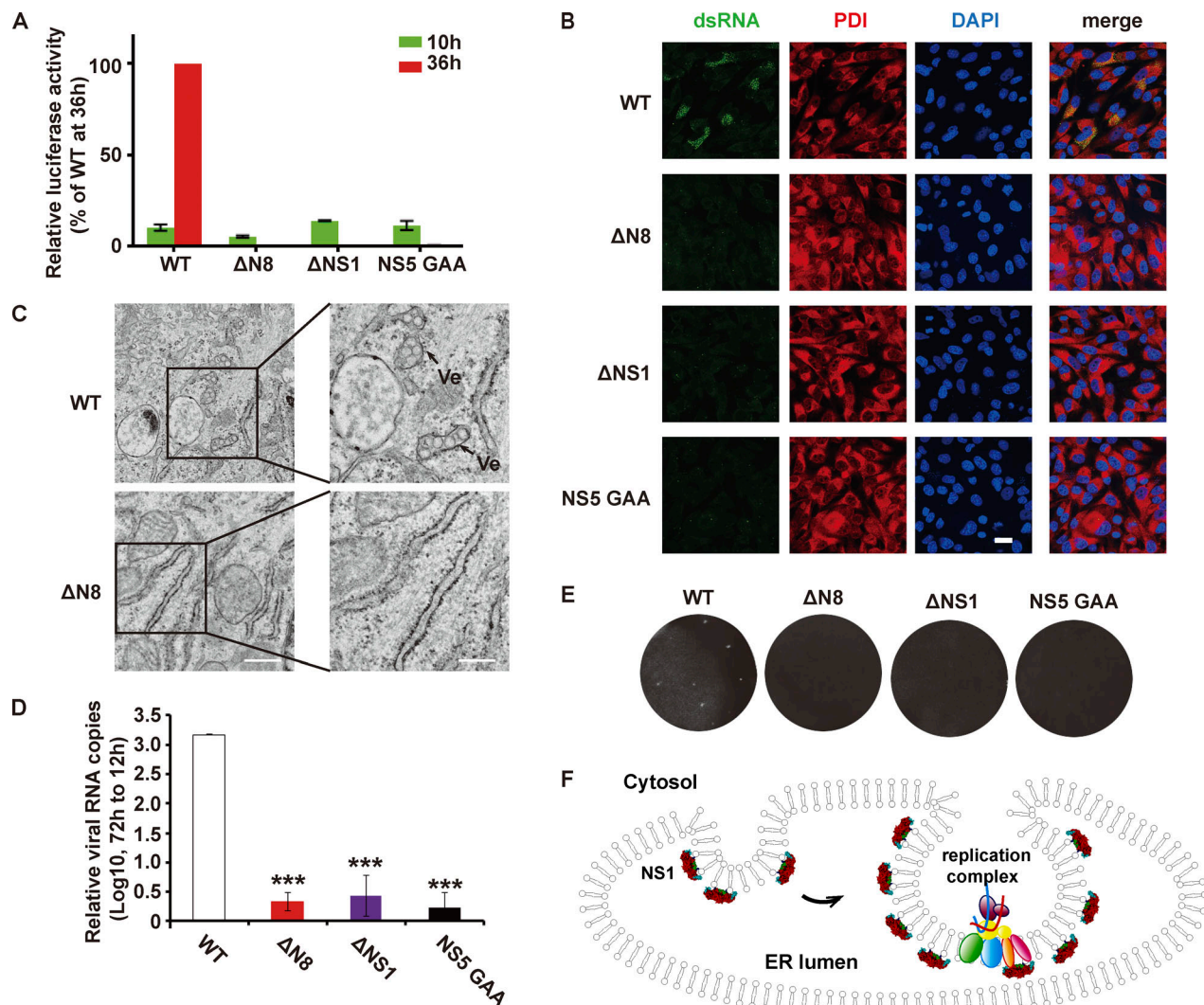


Figure 6. ZIKV NS1 is essential for viral replication relying on ER remodeling. (A) Luciferase activity of the ZIKV replicon. *Renilla* luciferase activity was measured at 10 h and 36 h after transfection of cells with WT or mutated ZIKV replicon RNA. (B) dsRNA intermediate staining in replicon-transfected cells. WT or mutated replicon-transfected BHK-21 cells were stained with J2 antibody (green, dsRNA specific antibody) and anti-PDI antibody (red, ER marker). Scale bar, 20 μ m. (C) EM images showing the ER structure in ZIKV replicon-transfected BHK-21 cells. Right panel: High-magnification image of the indicated area. Scale bars, 500 nm (left panel), 250 nm (right panel). (D) rZIKV production by WT or mutated infectious ZIKV RNA transcript. Fold change of the viral RNA copy number in the culture medium at 72 h relative to that at 12 h after transfection of cells with WT or mutated infectious ZIKV RNA transcript. The data are presented as the mean \pm SEM. The P values are obtained from a two-tailed t test. ***, $P < 0.001$. (E) Plaque assay to examine the infectivity of rZIKV. Vero cells were infected with equal amounts of 10-fold diluted WT or mutated rZIKV. A plaque assay was performed on day 5 after infection. (F) Schematic diagram of the ZIKV NS1-induced replication compartment formed by ER remodeling. ER lumen-localized ZIKV NS1 induces ER invagination through hydrophobic insertion into the inner leaflet of the ER membrane. Then, the invaginated vesicles become a platform for replication complex assembly and RNA synthesis.

connects with the cytoplasm to enable the import of materials and the export of products. To build these replication compartments, positive-strand RNA viruses must remodel the membrane to an ideal architecture. Many questions and disputes concerning the formation of the replication compartments exist. Previous studies have reported some potential viral or host proteins that might be involved in the biogenesis of replication compartments, such as the poliovirus 2C protein, and the host factors ADP-ribosylation factor and guanine nucleotide exchange factor (Belov et al., 2007; Cho et al., 1994).

As positive-strand RNA viruses, flaviviruses build replication compartments at the ER. Earlier studies suggested that viral

NS4A/B and host reticulon 3.1A have the potential to induce membrane alteration (Aktepe et al., 2017; Miller et al., 2007; Roosendaal et al., 2006; Stern et al., 2013). Our finding shows that the structure of ER induced by viral polypeptide NS2A-4B is quite different from that of the replication compartment. In fact, we found that NS1 is indispensable for the replication compartment biogenesis; NS1 alone is sufficient to induce ER remodeling with architecture similar to replication compartments. Previous studies unraveled genetic and/or physical interaction of NS1 with NS4A and NS4B; however, it was recently reported that this interaction had no relationship with the formation of the replication compartment (Lindenbach and Rice, 1999;

Plaszczyca et al., 2019; Youn et al., 2012). Thus, it is possible that ER lumen-localized NS1 regulates flavivirus replication via remodeling the ER structure or organizing the assembly of replication complexes. Of course, we cannot rule out the possibility that other NS proteins also participate in this process. One member of the genus *Hepacivirus* in the Flaviviridae family, hepatitis C virus (HCV), shares some properties with flaviviruses but has different replication compartments of double-membrane vesicles protruding from the ER (exvagination; Paul and Bartenschlager, 2015; Reiss et al., 2011). These double-membrane vesicles are considered to be induced by the viral protein NS4B through its N-terminal amphipathic helix (Elazar et al., 2004; Gouttenoire et al., 2014). Notably, unlike flaviviruses, HCV has no NS1-like protein that localizes in the ER lumen (Niepmann, 2013; Paul et al., 2014). The absence of such a protein might be one reason to explain the difference of the replication compartment between HCV and flaviviruses.

Membrane-remodeling mechanisms

Membrane remodeling is involved in many physiological processes, such as cell migration, division, organelle homeostasis, and vesicle trafficking. Membrane shape can be modulated by reversible insertion of proteins, oligomerization of scaffold proteins, and changes in lipid composition (McMahon and Gallop, 2005). Generally, membrane remodeling requires interactions between proteins and lipids, such as hydrophobic or electrostatic interaction. For example, the epsin N-terminal homology domain and N-BAR domain induce membrane curvature in an amphipathic helix-dependent manner (Frost et al., 2009). The C1 and C2 domains remodel the membrane via hydrophobic insertion and also require metal ions (Martens et al., 2007). Other domains, such as the PH, FYVE, and PX domains, can recognize specific phosphatidylinositol phosphates, providing targeting specificity and enhancing binding activity alone or in combination with other membrane-binding domains (Hurley, 2006).

The flavivirus NS1 protein remodels the ER using a different strategy. As the first NS protein to be translated, NS1 localizes to the ER lumen and binds to the inner leaflet of the ER membrane. Three hydrophobic regions protruding from the membrane-binding face provide five isolated but nearby insertion sites for a NS1 dimer. The hydrophobic region is either a β -roll or flexible loop rather than amphipathic helices, suggesting a distinct mechanism to change the membrane curvature. This multivalent insertion into the inner leaflet of the ER membrane can easily induce ER invagination.

A model for the biogenesis of NS1-induced viral replication compartments

Flaviviruses enter cells through endocytosis; then, the envelope protein mediates viral envelope fusion with the endosome membrane to release viral genome. The positive-strand viral RNA genome is translated into a polyprotein precursor on the ER membrane and then processed by host signal peptidase and viral NS3 protease. The NS1 protein is released from the polyprotein through cleavage by signal peptidase. ER lumen-localized NS1 induces ER invagination via hydrophobic insertion into the

inner leaflet of the ER membrane. Thus, flaviviruses build the replication compartment, which is the structural basis for subsequent replication complex assembly and viral RNA synthesis (Fig. 6 F). To further explore the role of NS1 in the formation of replication compartments, a cryo-EM study may elucidate NS1 organization on the lipid membrane, and live-cell imaging may provide kinetic information about NS1-induced ER remodeling.

Materials and methods

Cell culture

Human embryonic kidney cells HEK293T (ATCC CRL3216), human HeLa (ATCC CCL-2), African Green Monkey kidney cells Vero (ATCC CCL-81), and human glioblastoma cells U251 (ATCC CRL3216) were grown at 37°C with 5% CO₂ in DMEM supplemented with 10% FBS. The baby hamster kidney fibroblast cells BHK-21 (ATCC CCL10) were grown at 37°C with 5% CO₂ in DMEM supplemented with 5% FBS.

Antibodies

Antibodies used in this study include ZIKV NS1 (BioFront, BF-1225-36), ZIKV envelope protein (BioFront, BF-1176-56), Calreticulin (Abcam, ab2907 for HeLa and U251 cells, ab92516 for Vero cells), Myc-tag (MBL, M192-3), Flag-tag (Cell Signaling Technology, 14793), dsRNA-J2 (Scicons), β -actin (Sigma-Aldrich, A5441), Cy3-conjugated goat anti-rabbit (Jackson Immuno Research), and Alexa Fluor 488-conjugated Goat anti-mouse (Invitrogen).

Immunofluorescence microscopy

Cells were seeded on glass coverslips in 24-well plates and then transfected with the indicated plasmids. At 24 h after transfection, cells were fixed with 4% PFA at 37°C for 10 min and then washed with PBS buffer three times. The fixed cells were permeabilized with 0.2% Triton X-100 dissolved in PBS buffer for 10 min and then blocked with 3% BSA diluted in PBS buffer for 30 min at room temperature. The primary antibody incubation was performed at 37°C for 2 h. After rinsing with PBS buffer three times, cells were incubated with secondary antibody at 37°C for 1 h. Then cells were stained with 1 μ g/ml DAPI for 5 min. After washing three times, coverslips were mounted for image analysis under a Zeiss LSM780 confocal microscope.

Clone construction

pcDNA3.1-ss-Myc NS1 were constructed based on a flipped Myc-Syntaxin plasmid (gifted by J.E. Rhothman, Yale University, New Haven, CT), which was carrying an N-terminal bovine prolactin signal peptide sequence and Myc sequence. The EcoRV and XhoI restriction sites were introduced before and after Syntaxin coding sequence by site-directed mutagenesis. Then ZIKV NS1 was cloned into the flipped vector by restriction enzyme digestion and ligation strategy. ZIKV NS1 without signal sequence was prepared by inserting the NS1 sequence between XhoI/XbaI sites of pcDNA6. Similarly, DENV NS1 was cloned into EcoRV/XhoI sites of pcDNA3.1-ss-Myc vector, and DENV NS1 without signal sequence was cloned into pcDNA6 vector with XhoI/XbaI sites.

Protein expression and purification

HEK293T cells were transfected with pcDNA3.1-ss-NS1-6His (WT or mutants), and media were refreshed with Opti-MEM 24 h after transfection. After another 48-h culture, the media were collected and centrifuged at 4,000 rpm for 10 min to remove cell debris. The soluble NS1 proteins with His-tag that secreted into the media were purified by nickel-magnetic beads (Selleck). Protein-bound beads were collected and rinsed with wash buffer (100 mM NaCl, 50 mM Tris, and 20–50 mM imidazole, pH 7.5). Then the proteins were eluted by elution buffer (100 mM NaCl, 50 mM Tris, and 500 mM imidazole, pH 7.5).

ER luminal ZIKV NS1 was purified from HEK293T cell lysate. Transfection and protein expression were performed as described above. Then cells were washed with PBS buffer and lysed by lysis buffer (100 mM NaCl, 50 mM Tris, 0.5% Triton X-100, 0.6 mM DTT, 1 µg/ml Pepstatin, 1 µg/ml Aprotinin, 1 µg/ml Leupeptin, and 1 mM PMSF). Cell lysate was sonicated five times (5 s/time at 200 W) and then centrifuged (15,000 rpm) at 4°C for 15 min. The purification of protein was performed as described above.

Liposome preparation

Liposomes were prepared based on extrusion protocol as described (Berger et al., 2001). Briefly, cholesterol (Sigma-Aldrich, C8667) and 1,2-dioleoyl-sn-glycero-3-phosphocholine (Avanti, 850375) were mixed in 100 µl chloroform at molar ratios of 1:9 cholesterol:1,2-dioleoyl-sn-glycero-3-phosphocholine. Then the lipids mixture was dried under nitrogen gas and vacuumed for 2 h to remove chloroform. Lipids were resuspended with 800 µl buffer (100 mM NaCl and 50 mM Tris, pH 7.5) and vortexed at RT for 30 min. The resuspended mixture was subjected to seven freeze-thaw cycles and then extruded through a 100 nm or 400 nm polycarbonate membrane filter (Whatman, 610005 and 610009) with the Avanti Mini-Extruder (Avanti) at RT to prepare liposomes.

Liposome cofloating assay

Liposome cofloating assay was performed as previously described (Shen et al., 2007; Tucker et al., 2004). 40 µl of 100-nm liposomes were incubated with 40 µg NS1 proteins at 37°C for 4 h. Then the liposome-protein (add 70 µl buffer to 150 µl) mixture was mixed with an equal amount of 80% Nycodenz (wt/vol) diluted in buffer (100 mM NaCl and 50 mM Tris, pH 7.5) to get 40% Nycodenz mixture. Nycodenz gradients were assembled in 5 × 41 mm ultra-centrifuge tubes (Beckman, 344090) with 300 µl 40% Nycodenz-liposome-protein mixture in the bottom followed by 250 µl 30% Nycodenz and then 50 µl buffer (without Nycodenz) as the top layer. Each tube was subjected to centrifugation at 45,000 rpm in a MLS 50 rotor (Beckman) for 4 h. After centrifugation, 75 µl (37.5 µl each time, two times) liposomes were collected from the top, and samples were analyzed by SDS-PAGE and silver stain.

Doxyl-labeled lipid quenching assay

150 µM doxyl-labeled or unlabeled liposomes were mixed with 3 µM peptides, and the intensity of fluorescence was measured at an excitation wavelength of 280 nm and emission wavelength

of 330 nm by Thermo Varioskan Flash. Trp fluorescence intensity was detected when peptides were mixed with doxyl-labeled (F) or unlabeled (F0) liposome. The change of fluorescence intensity was indicated as F0/F.

Liposome-negative staining

400 nm liposomes were prepared as described above. Then liposomes were centrifuged at 13,000 rpm for 30 min to remove smaller ones. Liposome pellets were resuspended by buffer (100 mM NaCl and 50 mM Tris, pH 7.5). 10 µl liposomes were incubated with or without 6.4 µl 3 mg/ml NS1 proteins at RT for 2 h. 4.5 µl liposome-protein mixture was loaded on the copper grid for 1 min. The liquid was removed, and liposomes were stained with 2% uranyl acetate for 1 min. The rest of the uranyl acetate was removed, and the liposomes were air-dried for several minutes.

Liposome remodeling statistics

The length of each tube on a liposome was measured by ImageJ. Tubules with a length <500 nm were excluded as the background based on the native tubes present on liposomes alone. More than 200 liposomes were calculated.

APEX-tag staining

HeLa cells were seeded into a 35-mm culture dish and transfected with plasmids as indicated. At 24 or 36 h after transfection, cells were fixed by 2% glutaraldehyde solution in sodium cacodylate buffer on ice for 1 h. Cells were washed five times by sodium cacodylate buffer for 2 min each time. Then 20 mM glycine solution was added to block glutaraldehyde reaction for 5 min. After washing five times, cells were incubated with 0.5 mg/ml DAB solution in sodium cacodylate buffer for 1 h on ice followed by 0.5 mg/ml DAB/10 mM H₂O₂ solution incubation until the DAB reaction was visible. The DAB/H₂O₂ solution was removed, and cells were washed with sodium cacodylate buffer five times.

Post-fixation staining was performed with 2% osmium tetroxide for 5 min. After washing with distilled water three times for 5 min, cells were incubated in 2% aqueous uranyl acetate (Electron Microscopy Sciences, 22400) overnight. After washing by distilled water, cells were dehydrated in a graded ethanol series (50%, 70%, 80%, 90%, 100%, and 100%) for 2 min. After a final incubation in 100% ethanol for 2 min at room temperature, cells were infiltrated and embedded in Pon 812 resin. DAB-stained areas of embedded cells were identified by transmitted light, and the regions of interest were cut out using a razor blade and mounted on resin blocks with cyanoacrylic adhesive. The blocks were trimmed, and 70-nm ultrathin sections were cut. The middle depth sections were placed on copper grids and examined by transmission EM (Hitachi, H7650). We obtained data of ~20 cells for statistical analysis.

EM

EM was performed at the Center of Biomedical Analysis, Tsinghua University. ER morphology was observed by transmission EM. The culture cells that were grown on 35-mm dishes were fixed by 2.5% glutaraldehyde in PB buffer. After washing

with PB buffer, cells were post-fixed with 1% osmium containing 1.5% potassium ferrocyanide. Then cells were dehydrated with gradient ethanol (50%, 70%, 90%, 95%, and 100%). Samples were infiltrated with and embedded in SPON812 resin. After polymerizing, embedded monolayer samples were oriented cut to 70-nm-thick ultrathin sections by a diamond knife. The middle depth sections were picked up with copper grids and double-stained with uranyl acetate and lead citrate. After air drying, samples were observed with electron microscope H-7650. We observed ~20 cells for every experiment.

Immunoprecipitation

Myc- and Flag-tagged ZIKV NS1 cotransfected HEK293T cells were lysed with Pierce IP Lysis Buffer (Thermo Fisher Scientific, 87787) with protease inhibitors on ice for 10 min. The lysate was centrifuged (13,000 rpm) at 4°C for 10 min. The supernatant was incubated with anti-Myc (MBL) antibody for 2 h followed by incubation with protein A/G agarose beads (Santa Cruz Biotechnology, sc-2003) for 4 h at 4°C. After washing three times with IP Lysis buffer, the protein A/G agarose beads were re-suspended in 1× SDS protein loading buffer and boiled for 5 min. Then protein samples were analyzed by Western blot.

Western blot

Protein samples were submitted to SDS-PAGE and then transferred onto a nitrocellulose membrane. Proteins on the nitrocellulose membrane were immunoblotted with 1:5,000 diluted anti-Myc antibody (MBL, M193-3), 1:1,000 diluted anti-Flag antibody (Cell Signaling Technology, 14793), or 1:10,000 diluted anti-β-actin antibody (Sigma-Aldrich, A-5441) for 2 h at RT. After washing three times with 10 mM Tris, 150 mM NaCl, and 0.1% Tween 20, pH 7.6, the membrane was incubated with HRP-conjugated secondary antibody. Antibody-bound protein bands were detected by ECL plus Western blot system (Perkin Elmer).

ZIKV infection

The mammalian cells were seeded on glass coverslip in a 24-well plate. After 12 h, cells were infected with ZIKV (MOI 0.1 for Vero and U251 infection, MOI 1 for HeLa infection) for 2 h. Then the cells were cultured in DMEM for the indicated time and fixed for the experiments as mentioned above.

ZIKV replicon assay

ZIKV replicon assay was performed as previously described (Li et al., 2018). ZIKV replicon clone was kindly provided by B. Zhang at the Institute of Virology, Chinese Academy of Science, Wuhan, China. ZIKV replicon RNA was transcribed in vitro using the mMESSAGE mMACHINE T7 transcription kit (Thermo Fisher Scientific). 0.5 μg replicon RNA transcripts were transfected into 4 × 10⁴ BHK-21 cells (48-well plate) by 1.5 μl viafect transfect reagent (Promega). Transfected cell lysate was collected 10 h after transfection and 36 h after transfection. *Renilla reniformis* luciferase activity was measured by *Renilla* luciferase assay system (Promega).

rZIKV preparation

rZIKV was prepared by infectious DNA clone pACNR-GZ01 as previously described (Liu et al., 2017b). The whole genome

sequence was amplified in vitro by high-fidelity PCR, and the original SP6 promoter was replaced by a T7 promoter. The PCR products were purified by phenol-chloroform extraction and ethanol precipitation. The mMESSAGE mMACHINE T7 transcription kit (Ambion, Thermo Fisher Scientific) was used for in vitro RNA transcription. The reaction mixture was incubated at 37°C for 4 h followed by 30 min digestion with RNase-free DNase I. The RNA transcripts were purified by RNAfast200 kit (FASTAGEN). RNA products were then mixed with 2× splicing buffer (80 mM Tris-HCl, pH 7.4, 2 M NH₄Cl, 20 mM MgCl₂, and 0.04% sodium dodecyl sulfate) and incubated at 45°C for 1 h to remove intron. Secondary RNA purification was performed by RNAfast200 kit. 1.5 μg RNA products were transfected into 8 × 10⁴ BHK-21 cells seeded in a 24-well plate by 4.5 μl Viafect transfection reagent (Promega). At different time points, culture media were collected and stored at -80°C for subsequent viral infection experiments or RNA purification and quantitative PCR analysis (TIANGEN). pFLZIKV were used to construct mutated rZIKV. Full-length genome sequence was amplified by PCR. RNA transcription was performed by mMESSAGE mMACHINE T7 transcription kit (Ambion, Thermo Fisher Scientific). The products were purified by RNAfast200 kit (FASTAGEN).

Plaque assay

Viral stocks were 10-fold serially diluted in DMEM containing 2% FBS. For each dilution, 900 μl was added to Vero cells in a 12-well plate. After 2 h incubation, medium containing virus was discarded, and 2 ml of 1% low-melting agarose was added into each well. Then the plate was incubated at 37°C for 5 d. The infected cells were fixed with 4% formaldehyde for 1 h, followed by 1 h staining with 1% crystal violet. Visible plaques were counted, and viral infection efficiencies were calculated.

Statistical analysis and validations

The statistical significance was determined by two-tailed *t* test in all experiments. A minimum of three biological repeats was performed for each experiment. A minimum of 600 cells was counted over three repeats for percentage analysis in immunostaining experiments.

Online supplemental material

Fig. S1 shows the ultrastructure of ER in ZIKV-infected HeLa cells (A), BHK cells (B), and the ER network in ZIKV NS5-transfected cells (C). Fig. S2 displays the ER aggregation induced by DENV NS1. Fig. S3 A shows the sequence conservation of NS1 hydrophobic regions among flavivirus family members. Fig. S3, B and C, shows the expression and purification of NS1 mutants. Fig. S4 shows the cofloating assay of NS1 V6A and F8A mutants. Fig. S5 shows the luciferase activity of ZIKV replicons with point mutations in NS1.

Acknowledgments

We thank Dr. Frederic Pincet (Statistical Physics Laboratory of the Ecole Normale Supérieure, Paris, France) and Dr. Sandra Schmid (University of Texas Southwestern Medical Center, Dallas, TX) for reviewing and revising the manuscript. We

would like to thank Dr. Peiyong Shi (The University of Texas Medical Branch, Gavelston, TX) for kindly providing ZIKV infectious DNA clone and Dr. Bo Zhang (Institute of Virology, Chinese Academy of Sciences, Wuhan, China) for providing ZIKV replicon clone. We thank Ying Li and Xiaofeng Hu at the Tsinghua University Branch of the China National Center for Protein Sciences Beijing for technical support in preparing ultrathin sections and EM image acquisition.

We appreciate funding from the National Natural Science Foundation of China (81622028 and 31470813 to L. Shi; 81925003 and 31770190 to C.F. Qin), the 1000 Talents Plan Youth program (to L. Shi), the Chinese Academy of Medical Sciences Innovation Fund for Medical Sciences (2016-I2M-3-020), and the Chinese Academy of Medical Sciences (2016ZX310192, 2016RC310037, and 2016RC310031) to support the project.

The authors declare no competing financial interests.

Author contributions: Y. Ci, Z.Y. Liu, N.N. Zhang, Y. Niu, and Y. Yang performed experiments. Y. Ci, C. Xu, W. Yang, C.F. Qin, and L. Shi designed the project and analyzed data. Y. Ci and L. Shi wrote the manuscript together with all other authors.

Submitted: 18 March 2019

Revised: 29 September 2019

Accepted: 8 November 2019

References

- Akey, D.L., W.C. Brown, S. Dutta, J. Konwerski, J. Jose, T.J. Jurkiw, J. Del-Proposto, C.M. Ogata, G. Skiniotis, R.J. Kuhn, and J.L. Smith. 2014. Flavivirus NS1 structures reveal surfaces for associations with membranes and the immune system. *Science*. 343:881–885. <https://doi.org/10.1126/science.1247749>
- Aktepe, T.E., S. Liebscher, J.E. Prier, C.P. Simmons, and J.M. Mackenzie. 2017. The Host Protein Reticulon 3.1A Is Utilized by Flaviviruses to Facilitate Membrane Remodelling. *Cell Reports*. 21:1639–1654. <https://doi.org/10.1016/j.celrep.2017.10.055>
- Apte-Sengupta, S., D. Sirohi, and R.J. Kuhn. 2014. Coupling of replication and assembly in flaviviruses. *Curr. Opin. Virol.* 9:134–142. <https://doi.org/10.1016/j.coviro.2014.09.020>
- Belov, G.A., C. Habbersett, D. Franco, and E. Ehrenfeld. 2007. Activation of cellular Arf GTPases by poliovirus protein 3CD correlates with virus replication. *J. Virol.* 81:9259–9267. <https://doi.org/10.1128/JVI.00840-07>
- Berger, N., A. Sachse, J. Bender, R. Schubert, and M. Brandl. 2001. Filter extrusion of liposomes using different devices: comparison of liposome size, encapsulation efficiency, and process characteristics. *Int. J. Pharm.* 223:55–68. [https://doi.org/10.1016/S0378-5173\(01\)00721-9](https://doi.org/10.1016/S0378-5173(01)00721-9)
- Brown, W.C., D.L. Akey, J.R. Konwerski, J.T. Tarrasch, G. Skiniotis, R.J. Kuhn, and J.L. Smith. 2016. Extended surface for membrane association in Zika virus NS1 structure. *Nat. Struct. Mol. Biol.* 23:865–867. <https://doi.org/10.1038/nsmb.3268>
- Chambers, T.J., C.S. Hahn, R. Galler, and C.M. Rice. 1990. Flavivirus genome organization, expression, and replication. *Annu. Rev. Microbiol.* 44: 649–688. <https://doi.org/10.1146/annurev.mi.44.100190.003245>
- Chen, J., M.M. Ng, and J.J. Chu. 2015. Activation of TLR2 and TLR6 by Dengue NS1 Protein and Its Implications in the Immunopathogenesis of Dengue Virus Infection. *PLoS Pathog.* 11:e1005053. <https://doi.org/10.1371/journal.ppat.1005053>
- Cho, M.W., N. Teterina, D. Egger, K. Bienz, and E. Ehrenfeld. 1994. Membrane rearrangement and vesicle induction by recombinant poliovirus 2C and 2BC in human cells. *Virology*. 202:129–145. <https://doi.org/10.1006/viro.1994.1329>
- Cortese, M., S. Goellner, E.G. Acosta, C.J. Neufeldt, O. Oleksiuk, M. Lampe, U. Haselmann, C. Funaya, N. Schieber, P. Ronchi, et al. 2017. Ultrastructural Characterization of Zika Virus Replication Factories. *Cell Reports*. 18:2113–2123. <https://doi.org/10.1016/j.celrep.2017.02.014>
- den Boon, J.A., and P. Ahlquist. 2010. Organelle-like membrane compartmentalization of positive-strand RNA virus replication factories. *Annu. Rev. Microbiol.* 64:241–256. <https://doi.org/10.1146/annurev.micro.112408.134012>
- Elazar, M., P. Liu, C.M. Rice, and J.S. Glenn. 2004. An N-terminal amphipathic helix in hepatitis C virus (HCV) NS4B mediates membrane association, correct localization of replication complex proteins, and HCV RNA replication. *J. Virol.* 78:11393–11400. <https://doi.org/10.1128/JVI.78.20.11393-11400.2004>
- Frost, A., V.M. Unger, and P. De Camilli. 2009. The BAR domain superfamily: membrane-molding macromolecules. *Cell*. 137:191–196. <https://doi.org/10.1016/j.cell.2009.04.010>
- Fulton, B.O., D. Sachs, M.C. Schwarz, P. Palese, and M.J. Evans. 2017. Transposon Mutagenesis of the Zika Virus Genome Highlights Regions Essential for RNA Replication and Restricted for Immune Evasion. *J. Virol.* 91:e00698–17. <https://doi.org/10.1128/JVI.00698-17>
- Glasner, D.R., H. Puerta-Guardo, P.R. Beatty, and E. Harris. 2018. The Good, the Bad, and the Shocking: The Multiple Roles of Dengue Virus Non-structural Protein 1 in Protection and Pathogenesis. *Annu. Rev. Virol.* 5: 227–253. <https://doi.org/10.1146/annurev-virology-101416-041848>
- Gouttenoire, J., R. Montserret, D. Paul, R. Castillo, S. Meister, R. Bartenschlager, F. Penin, and D. Moradpour. 2014. Aminoterminal amphipathic α -helix AH1 of hepatitis C virus nonstructural protein 4B possesses a dual role in RNA replication and virus production. *PLoS Pathog.* 10:e1004501. <https://doi.org/10.1371/journal.ppat.1004501>
- Gutsche, I., F. Coulbaly, J.E. Voss, J. Salmon, J. d'Alayer, M. Ermonval, E. Larquet, P. Charneau, T. Krey, F. M  gret, et al. 2011. Secreted dengue virus nonstructural protein NS1 is an atypical barrel-shaped high-density lipoprotein. *Proc. Natl. Acad. Sci. USA*. 108:8003–8008. <https://doi.org/10.1073/pnas.1017338108>
- Hsu, N.Y., O. Ilnytska, G. Belov, M. Santiana, Y.H. Chen, P.M. Takvorian, C. Pau, H. van der Schaar, N. Kaushik-Basu, T. Balla, et al. 2010. Viral reorganization of the secretory pathway generates distinct organelles for RNA replication. *Cell*. 141:799–811. <https://doi.org/10.1016/j.cell.2010.03.050>
- Hurley, J.H. 2006. Membrane binding domains. *Biochim. Biophys. Acta*. 1761: 805–811. <https://doi.org/10.1016/j.bbali.2006.02.020>
- Jarsch, I.K., F. Daste, and J.L. Gallop. 2016. Membrane curvature in cell biology: An integration of molecular mechanisms. *J. Cell Biol.* 214:375–387. <https://doi.org/10.1083/jcb.201604003>
- Li, J.Q., C.L. Deng, D. Gu, X. Li, L. Shi, J. He, Q.Y. Zhang, B. Zhang, and H.Q. Ye. 2018. Development of a replicon cell line-based high throughput antiviral assay for screening inhibitors of Zika virus. *Antiviral Res.* 150: 148–154. <https://doi.org/10.1016/j.antiviral.2017.12.017>
- Lindenbach, B.D., and C.M. Rice. 1997. trans-Complementation of yellow fever virus NS1 reveals a role in early RNA replication. *J. Virol.* 71: 9608–9617.
- Lindenbach, B.D., and C.M. Rice. 1999. Genetic interaction of flavivirus nonstructural proteins NS1 and NS4A as a determinant of replicase function. *J. Virol.* 73:4611–4621.
- Liu, Y., J. Liu, S. Du, C. Shan, K. Nie, R. Zhang, X.F. Li, R. Zhang, T. Wang, C.F. Qin, et al. 2017a. Evolutionary enhancement of Zika virus infectivity in *Aedes aegypti* mosquitoes. *Nature*. 545:482–486. <https://doi.org/10.1038/nature22365>
- Liu, Z.Y., J.Y. Yu, X.Y. Huang, H. Fan, X.F. Li, Y.Q. Deng, X. Ji, M.L. Cheng, Q. Ye, H. Zhao, et al. 2017b. Characterization of cis-Acting RNA Elements of Zika Virus by Using a Self-Splicing Ribozyme-Dependent Infectious Clone. *J. Virol.* 91:e00484–17. <https://doi.org/10.1128/JVI.00484-17>
- Ma, W., S. Li, S. Ma, L. Jia, F. Zhang, Y. Zhang, J. Zhang, G. Wong, S. Zhang, X. Lu, et al. 2017. Zika Virus Causes Testis Damage and Leads to Male Infertility in Mice. *Cell*. 168:542. <https://doi.org/10.1016/j.cell.2017.01.009>
- Martens, S., M.M. Kozlov, and H.T. McMahon. 2007. How synaptotagmin promotes membrane fusion. *Science*. 316:1205–1208. <https://doi.org/10.1126/science.1142614>
- McMahon, H.T., and J.L. Gallop. 2005. Membrane curvature and mechanisms of dynamic cell membrane remodelling. *Nature*. 438:590–596. <https://doi.org/10.1038/nature04396>
- Miller, E.A., and C. Barlowe. 2010. Regulation of coat assembly--sorting things out at the ER. *Curr. Opin. Cell Biol.* 22:447–453. <https://doi.org/10.1016/j.ccb.2010.04.003>
- Miller, S., S. Kastner, J. Krijnse-Locker, S. B  hler, and R. Bartenschlager. 2007. The non-structural protein 4A of dengue virus is an integral membrane protein inducing membrane alterations in a 2K-regulated

- manner. *J. Biol. Chem.* 282:8873–8882. <https://doi.org/10.1074/jbc.M609919200>
- Muyllaert, I.R., R. Galler, and C.M. Rice. 1997. Genetic analysis of the yellow fever virus NS1 protein: identification of a temperature-sensitive mutation which blocks RNA accumulation. *J. Virol.* 71:291–298.
- Niepmann, M. 2013. Hepatitis C virus RNA translation. *Curr. Top. Microbiol. Immunol.* 369:143–166.
- Paul, D., and R. Bartenschlager. 2015. Flaviviridae Replication Organelles: Oh, What a Tangled Web We Weave. *Annu. Rev. Virol.* 2:289–310. <https://doi.org/10.1146/annurev-virology-100114-055007>
- Paul, D., V. Madan, and R. Bartenschlager. 2014. Hepatitis C virus RNA replication and assembly: living on the fat of the land. *Cell Host Microbe.* 16:569–579. <https://doi.org/10.1016/j.chom.2014.10.008>
- Plaszczycza, A., P. Scaturro, C.J. Neufeldt, M. Cortese, B. Cerikan, S. Ferla, A. Brancale, A. Pichlmair, and R. Bartenschlager. 2019. A novel interaction between dengue virus nonstructural protein 1 and the NS4A-2K-4B precursor is required for viral RNA replication but not for formation of the membranous replication organelle. *PLoS Pathog.* 15:e1007736. <https://doi.org/10.1371/journal.ppat.1007736>
- Ravindran, M.S., P. Bagchi, C.N. Cunningham, and B. Tsai. 2016. Opportunistic intruders: how viruses orchestrate ER functions to infect cells. *Nat. Rev. Microbiol.* 14:407–420. <https://doi.org/10.1038/nrmicro.2016.60>
- Reiss, S., I. Rebhan, P. Backes, I. Romero-Brey, H. Erfle, P. Matula, L. Kaderali, M. Poenisch, H. Blankenburg, M.S. Hiet, et al. 2011. Recruitment and activation of a lipid kinase by hepatitis C virus NS5A is essential for integrity of the membranous replication compartment. *Cell Host Microbe.* 9:32–45. <https://doi.org/10.1016/j.chom.2010.12.002>
- Roosendaal, J., E.G. Westaway, A. Khromykh, and J.M. Mackenzie. 2006. Regulated cleavages at the West Nile virus NS4A-2K-NS4B junctions play a major role in rearranging cytoplasmic membranes and Golgi trafficking of the NS4A protein. *J. Virol.* 80:4623–4632. <https://doi.org/10.1128/JVI.80.9.4623-4632.2006>
- Selisko, B., C. Wang, E. Harris, and B. Canard. 2014. Regulation of Flavivirus RNA synthesis and replication. *Curr. Opin. Virol.* 9:74–83. <https://doi.org/10.1016/j.coviro.2014.09.011>
- Shan, C., X. Xie, A.E. Muruato, S.L. Rossi, C.M. Roundy, S.R. Azar, Y. Yang, R.B. Tesh, N. Bourne, A.D. Barrett, et al. 2016. An Infectious cDNA Clone of Zika Virus to Study Viral Virulence, Mosquito Transmission, and Antiviral Inhibitors. *Cell Host Microbe.* 19:891–900. <https://doi.org/10.1016/j.chom.2016.05.004>
- Shen, J., D.C. Tareste, F. Paumet, J.E. Rothman, and T.J. Melia. 2007. Selective activation of cognate SNAREpins by Sec1/Munc18 proteins. *Cell.* 128:183–195. <https://doi.org/10.1016/j.cell.2006.12.016>
- Stern, O., Y.F. Hung, O. Valda, Y. Yaffe, E. Harris, S. Hoffmann, D. Willbold, and E.H. Sklan. 2013. An N-terminal amphipathic helix in dengue virus nonstructural protein 4A mediates oligomerization and is essential for replication. *J. Virol.* 87:4080–4085. <https://doi.org/10.1128/JVI.01900-12>
- Tang, H., C. Hammack, S.C. Ogden, Z. Wen, X. Qian, Y. Li, B. Yao, J. Shin, F. Zhang, E.M. Lee, et al. 2016. Zika Virus Infects Human Cortical Neural Progenitors and Attenuates Their Growth. *Cell Stem Cell.* 18:587–590. <https://doi.org/10.1016/j.stem.2016.02.016>
- Tucker, W.C., T. Weber, and E.R. Chapman. 2004. Reconstitution of Ca²⁺-regulated membrane fusion by synaptotagmin and SNAREs. *Science.* 304:435–438. <https://doi.org/10.1126/science.1097196>
- Watterson, D., N. Modhiran, and P.R. Young. 2016. The many faces of the flavivirus NS1 protein offer a multitude of options for inhibitor design. *Antiviral Res.* 130:7–18. <https://doi.org/10.1016/j.antiviral.2016.02.014>
- Welsch, S., S. Miller, I. Romero-Brey, A. Merz, C.K. Bleck, P. Walther, S.D. Fuller, C. Antony, J. Krijnse-Locker, and R. Bartenschlager. 2009. Composition and three-dimensional architecture of the dengue virus replication and assembly sites. *Cell Host Microbe.* 5:365–375. <https://doi.org/10.1016/j.chom.2009.03.007>
- Wikan, N., and D.R. Smith. 2016. Zika virus: history of a newly emerging arbovirus. *Lancet Infect. Dis.* 16:e119–e126. [https://doi.org/10.1016/S1473-3099\(16\)30010-X](https://doi.org/10.1016/S1473-3099(16)30010-X)
- Xu, X., H. Song, J. Qi, Y. Liu, H. Wang, C. Su, Y. Shi, and G.F. Gao. 2016. Contribution of intertwined loop to membrane association revealed by Zika virus full-length NS1 structure. *EMBO J.* 35:2170–2178. <https://doi.org/10.15252/embj.201695290>
- Youn, S., T. Li, B.T. McCune, M.A. Edeling, D.H. Fremont, I.M. Cristea, and M.S. Diamond. 2012. Evidence for a genetic and physical interaction between nonstructural proteins NS1 and NS4B that modulates replication of West Nile virus. *J. Virol.* 86:7360–7371. <https://doi.org/10.1128/JVI.00157-12>
- Yuan, L., X.Y. Huang, Z.Y. Liu, F. Zhang, X.L. Zhu, J.Y. Yu, X. Ji, Y.P. Xu, G. Li, C. Li, et al. 2017. A single mutation in the prM protein of Zika virus contributes to fetal microcephaly. *Science.* 358:933–936. <https://doi.org/10.1126/science.aam7120>